Magnetization, squeezing, and entanglement in dipolar spin-1 condensates

S. Yi[1,2] and H. Pu[1]
[1]*Department of Physics and Astronomy, and Rice Quantum Institute, Rice University, Houston, Texas 77251-1892, USA*
[2]*Institute of Theoretical Physics, The Chinese Academy of Science, Beijing, 100080, China*
(Received 28 October 2005; published 6 February 2006)

We study the static and dynamic responses of an $F=1$ dipolar spinor condensate with magnetic dipole moment under external magnetic fields, focusing on the effects induced by the magnetic dipolar interactions between atoms. A rich set of phenomena are investigated such as the ground state quantum phases, the magnetization steps, spin squeezing, and macroscopic entanglement generation.

DOI: 10.1103/PhysRevA.73.023602 PACS number(s): 03.75.Mn, 03.75.Gg, 75.45.+j, 75.60.Ej

I. INTRODUCTION

Since the experimental realizations of spinor condensates in ^{23}Na and ^{87}Rb atoms [1–3], their magnetic properties have been under intense experimental [2] and theoretical [4] studies. The short-range spin-exchange interaction, responsible for the formation of various magnetic phases [5,6], domain structure [2], and spin mixing dynamics [7,8], has been the focus of these studies. The long-range magnetic dipole-dipole interaction in alkali condensates, by contrast, has not received much attention. This stems from the fact that for ground state alkali atoms, the dipolar interaction strength is three orders of magnitude smaller than the s-wave collisional interaction strength. We, however, want to point out that the dipolar interaction may have a rather significant effect on alkali spinor condensates. This is due to the fact that, for both ^{23}Na and ^{87}Rb, the singlet and triplet s-wave scattering lengths (denoted by a_0 and a_2, respectively) are nearly equal. The short-range spin-exchange interaction depends on the difference of a_0 and a_2 [5,6], and hence has a strength much smaller than that of the total collisional interaction. A simple calculation shows that the magnitude of the dipolar interaction can be as large as 10% of the spin-exchange interaction for ^{87}Rb atoms [9], and the dipolar effects can be dramatically enhanced due to its long-range and anisotropic nature.

The dipolar effects in scalar condensates, where all dipole moments are polarized by an external field, have been studied extensively [10]. However, the magnetic properties associated with the spin degrees of freedom become manifest only when the magnetic dipole moments are unlocked, as in spinor condensates. In a series of work by Pu and co-workers [11], effects of dipolar interaction on spinor condensates confined in multi-well potentials are investigated. In those studies, only the dipolar coupling between atoms at different wells is taken into account, based on the assumption that the spin-exchange interaction dominates the intra-well interaction. The dipolar effects in a singly trapped spinor condensate in a magnetic field-free environment is investigated in Ref. [9].

In the present work, we consider a system of a singly trapped dipolar spin-1 condensate in weak magnetic fields, we shall focus on its static and dynamic magnetic responses, the ground state spin squeezing, and macroscopic entanglement generating. These studies show that dipolar spinor condensates exhibit a particularly rich spectrum of quantum magnetic behavior and thus represent a quantum magnetic system.

We remark that recent realization of the ^{52}Cr condensate [12] has attracted much attention on dipolar quantum gases as the ^{52}Cr atom boasts a much stronger dipolar interaction compared to its alkaline counterparts. However, due to the complexity of its ground state structure (the ^{52}Cr atom has total spin $S=3$ whose collisional interactions are characterized by four parameters, which are not all well known [13]), we shall consider the spin-1 system of ^{23}Na and ^{87}Rb condensates whose relative simplicity allows us to bring out the dipolar effects more clearly.

II. MODEL

We consider N condensed spin $F=1$ atoms trapped in an axially symmetric potential, $V_{\text{ext}}(\mathbf{r})$, with the symmetry axis chosen to be the quantization axis, $\hat{z}$. The atoms interact with each other via both short-range collisions and long-range magnetic dipolar interaction. Under a uniform magnetic field $\mathbf{B}$, the second quantized Hamiltonian of the system reads

$$\mathcal{H}=\mathcal{H}_0+\mathcal{H}_{\text{dd}}$$

where $\mathcal{H}_0$ and $\mathcal{H}_{\text{dd}}$ represent the nondipolar and dipolar part of the Hamiltonian, respectively, and are given by

$$\mathcal{H}_0=\int d\mathbf{r}\hat{\psi}_\alpha^\dagger(\mathbf{r})\left[\left(-\frac{\hbar^2\nabla^2}{2M}+V_{\text{ext}}(\mathbf{r})\right)\delta_{\alpha\beta}-g_F\mu_B\mathbf{B}\cdot\mathbf{F}_{\alpha\beta}\right]\hat{\psi}_\beta(\mathbf{r})+\frac{c_0}{2}\int d\mathbf{r}\hat{\psi}_\alpha^\dagger(\mathbf{r})\hat{\psi}_\beta^\dagger(\mathbf{r})\hat{\psi}_\alpha(\mathbf{r})\hat{\psi}_\beta(\mathbf{r})+\frac{c_2}{2}\int d\mathbf{r}\hat{\psi}_\alpha^\dagger(\mathbf{r})\hat{\psi}_{\alpha'}^\dagger(\mathbf{r})\mathbf{F}_{\alpha\beta}\cdot\mathbf{F}_{\alpha'\beta'}\hat{\psi}_\beta(\mathbf{r})\hat{\psi}_{\beta'}(\mathbf{r}),\tag{1}$$

$$\mathcal{H}_{\text{dd}}=\frac{c_d}{2}\int\int\frac{d\mathbf{r}d\mathbf{r}'}{|\mathbf{r}-\mathbf{r}'|^3}[\hat{\psi}_\alpha^\dagger(\mathbf{r})\hat{\psi}_{\alpha'}^\dagger(\mathbf{r}')\mathbf{F}_{\alpha\beta}\cdot\mathbf{F}_{\alpha'\beta'}\hat{\psi}_\beta(\mathbf{r})\hat{\psi}_{\beta'}(\mathbf{r}')-3\hat{\psi}_\alpha^\dagger(\mathbf{r})\hat{\psi}_{\alpha'}^\dagger(\mathbf{r}')\mathbf{F}_{\alpha\beta}\cdot\mathbf{e}\mathbf{F}_{\alpha'\beta'}\cdot\mathbf{e}\hat{\psi}_\beta(\mathbf{r})\hat{\psi}_{\beta'}(\mathbf{r}')],\tag{2}$$

where $\mathbf{e}=(\mathbf{r}-\mathbf{r}')/|\mathbf{r}-\mathbf{r}'|$ is a unit vector, M the mass of the atoms, and $\hat{\psi}_\alpha(\mathbf{r})$ the field operator for spin component α

$=1,0,-1$. The collisional interaction parameters are [5,6]

$$c_0 = \frac{4\pi\hbar^2(a_0+2a_2)}{3M}, \quad c_2 = \frac{4\pi\hbar^2(a_2-a_0)}{3M}.$$

The dipolar interaction parameter is

$$c_d = \frac{\mu_0 g_F^2 \mu_B^2}{4\pi},$$

with μ_0 being the vacuum magnetic permeability, g_F the Landé g-factor and μ_B the Bohr magneton. Finally, it is assumed in Eqs. (1) and (2) that the repeated indices are summed over.

For both the ^{87}Rb and ^{23}Na atoms, the interaction parameters are such that $|c_2| \ll c_0$ and $c_d \lesssim 0.1|c_2|$. Under these conditions, the single mode approximation (SMA) is expected to be valid, which allows us to decompose the field operator as [7,9,14]

$$\hat{\psi}_\alpha(\mathbf{r}) \simeq \phi(\mathbf{r})\hat{a}_\alpha, \tag{3}$$

with $\phi(\mathbf{r})$ being a spin-independent axially symmetric mode function and $\hat{a}_\alpha$ the annihilation operator of spin component α. Under the SMA, the Hamiltonian (with constant terms dropped) can be remarkably simplified as [9]

$$\mathcal{H} = (c_2' - c_d')\hat{\mathbf{L}}^2 + 3c_d'(\hat{L}_z^2 + \hat{n}_0) - g_F\mu_B \mathbf{B}\cdot\hat{\mathbf{L}}, \tag{4}$$

where $\hat{n}_0 = \hat{a}_0^\dagger \hat{a}_0$, $\hat{\mathbf{L}} = \Sigma_{\alpha\beta}\hat{a}_\alpha^\dagger \mathbf{F}_{\alpha\beta}\hat{a}_\beta$ is the total angular momentum operator and $\hat{L}_z$ is its z-component. The detailed derivation of the Hamiltonian (4) is provided in the Appendix. The rescaled collisional and dipolar interaction strengths are

$$c_2' = \frac{c_2}{2}\int d\mathbf{r}|\phi(\mathbf{r})|^4, \tag{5}$$

$$c_d' = \frac{c_d}{4}\int d\mathbf{r}\int d\mathbf{r}'|\phi(\mathbf{r})\phi(\mathbf{r}')|^2 \frac{1-3\cos^2\theta_{\mathbf{e}}}{|\mathbf{r}-\mathbf{r}'|^3}, \tag{6}$$

with $\theta_{\mathbf{e}}$ being the polar angle of the vector $(\mathbf{r}-\mathbf{r}')$. While the sign of c_2' is determined by the type of atoms: $c_2'>0$ (<0) for ^{23}Na (^{87}Rb), the sign and the magnitude of c_d' can be easily tuned by changing the trapping geometry: $c_d'>0$ (<0) for a pancake-shaped (cigar-shaped) condensate [9].

It is convenient to rescale Eq. (4) using $|c_2'|$ the units for energy (the corresponding units for time is then $\hbar/|c_2'|$), which yields the dimensionless Hamiltonian

$$\mathcal{H} = (\pm 1 - c)\hat{\mathbf{L}}^2 + 3c(\hat{L}_z^2 + \hat{n}_0) - \mathbf{H}\cdot\hat{\mathbf{L}}, \tag{7}$$

where $c \equiv c_d'/|c_2'|$, $\mathbf{H} = g_F\mu_B\mathbf{B}/|c_2'|$, and the sign "+" ("−") corresponds to $c_2>0$ (<0).

III. GROUND STATE STRUCTURE

Equation (7) is reminiscent of the Hamiltonian describing an anisotropic quantum magnet. As shown in Fig. 1, the $c_2'-c_d'$ parameter plane is divided into three regions (A, B, and C) based on the ground state wave function [9]. Regions A and B represent ferromagnetic phases with easy-plane and easy-axis anisotropy, respectively. In these two regions, the $\hat{n}_0$-term in Hamiltonian (7) can be neglected for $N \gg 1$, and the ground state stays in the $l=N$ angular momentum manifold. Region C represents roughly an anti-ferromagnetic phase. Here the $\hat{n}_0$-term cannot be neglected in general and will couple different angular momentum manifolds.

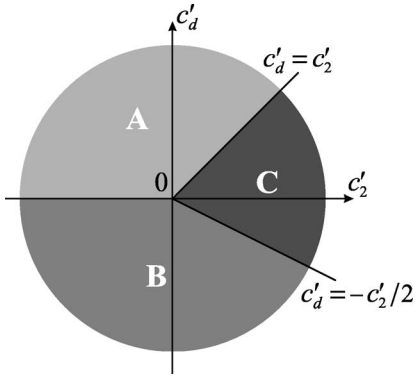

FIG. 1. Magnetic phases of dipolar spin-1 condensate. Region A and B corresponds to the ferromagnetic phases with, respectively, the in-plane and the uniaxial anisotropy. Region C represents roughly an anti-ferromagnetic phase.

First we consider the case that a field is applied longitudinally along the positive z-axis. In region A, the ground state takes the form $|N,m\rangle$ with $m=[(H/6c)+(1/2)]$ ($[x]$ denotes the largest integer less than or equal to x), where we have introduced the standard angular momentum basis state $|l,m\rangle$ that are common eigenstates of $\hat{\mathbf{L}}^2$ and $\hat{L}_z$. The atomic spins are fully polarized by the field (i.e., $m=N$) for $H > 6c(N-1/2)$. In real units, this field strength is on the order of 0.1 mG (1 mG) for typical Rb (Cr) condensate parameters. In the absence of the external field, the ground state in region B exhibits spontaneous magnetization with a twofold degeneracy $|N,\pm N\rangle$ [9]. This degeneracy is lifted by the longitudinal field and the state $|N,N\rangle$ is now the sole ground state. The ground state in region C has a general form of $\Sigma_{l\geq m_0} g_l|l,m_0\rangle$, where m_0 increases with the magnetic field and g_l has to be found numerically. In this region, the magnetization saturates at a field $H=(4N-5)c+2N-1$.

Next we apply the field transversely along the x-axis. Since xy-plane is the easy-plane for region A, the magnetization saturates under a transverse field of arbitrary strength. The ground state of region B can be understood classically. After dropping the unimportant $\hat{n}_0$-term and the constant $\hat{\mathbf{L}}^2$ (as $l=N$) terms, the classical version of the Hamiltonian (7) becomes

$$E(\vartheta) = 3cN^2\cos^2\vartheta - HN\sin\vartheta, \tag{8}$$

where ϑ is the polar angle of $\mathbf{L}$. The ground state ϑ_0 is obtained by minimizing the energy. For $H<-6cN$, $E(\vartheta)$ has two degenerate minima at

$$\vartheta_0^{(\pm)} = \frac{\pi}{2} \pm \left(\frac{\pi}{2} + \sin^{-1}\frac{H}{6cN}\right).$$

The degeneracy is removed when $H \geq -6cN$, for which the system is completely polarized by the external magnetic

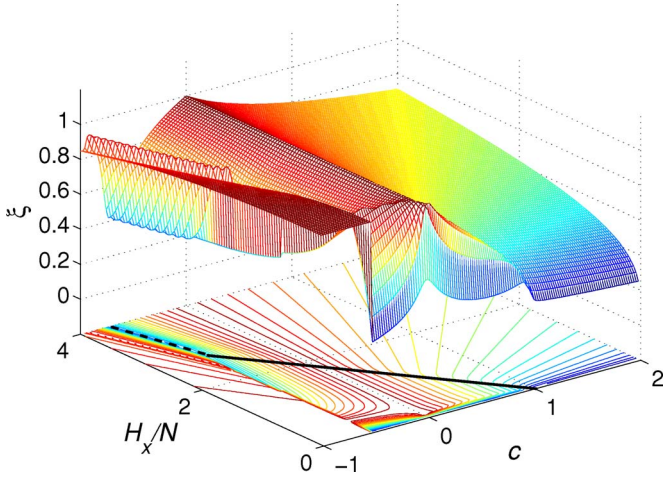

FIG. 2. (Color online) The squeezing parameter ξ as a function of transverse field H_x and c for $c_2>0$ and $N=40$. The dashed and solid lines on the contour plot represent the saturation field, which corresponds to the local minimum of ξ, in regions B and C, respectively.

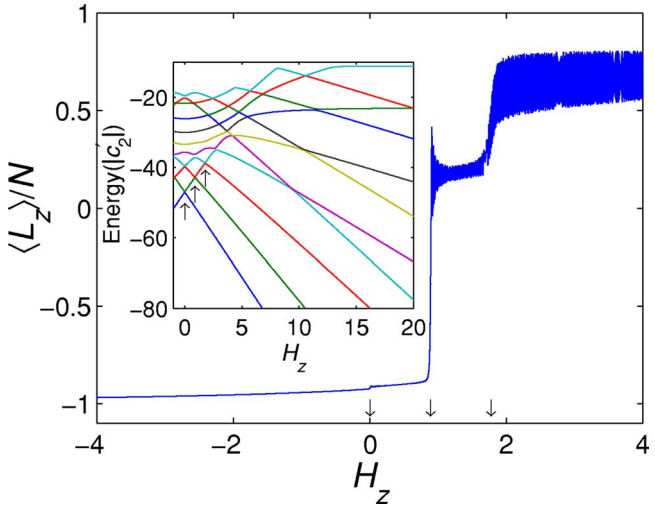

FIG. 3. (Color online) The dynamic response of the magnetization to a magnetic field sweep. The parameters we used here are $N=5$, $c=-0.33$, $H_x=3$, and $v=10^{-3}$, which represents a condensate in region B. The arrows denote the positions of the magnetization jumps. After the third jump, the amplitude of level $|N,-N\rangle$ in the condensate wave function is essentially zero, therefore, no more jumps are observed at higher field. The inset shows the energy spectrum as a function of applied longitudinal field H_z, the arrows in the inset mark the first three anti-crossings which match with the arrows in the main figure.

field. Hence $H_{\rm sat}=-6cN$ is the classical saturation field. Quantum mechanically, the degeneracy is lifted before the magnetic field reaches $H_{\rm sat}$ due to magnetization tunneling, a phenomenon studied extensively in the field of quantum magnetism [15]. The dipolar spinor condensate provides another system that exhibits such macroscopic quantum coherent behavior.

Finally, for region C, the ground state can only be obtained numerically as a superposition of different angular momentum states as in the previous case. The saturation field, however, has an analytic form $2(1-c)N$.

IV. SPIN SQUEEZING

A collective spin system is regarded as squeezed if the variance of one spin component normal to the mean spin vector is lower than the Heisenberg limited value. The spin squeezed state has important applications in ultra-precision measurement [16–19]. Mathematically, the criteria for spin squeezing is [17]

$$\xi \equiv \Delta L_< / \sqrt{|\langle \hat{\mathbf{L}} \rangle/2|} < 1,$$

with $\Delta L_<$ being the minimum fluctuation of a spin component perpendicular to the mean spin vector $\langle \hat{\mathbf{L}} \rangle$.

It can be easily shown that the ground state of Hamiltonian (7) with the magnetic field applied longitudinally does not exhibit spin squeezing. Spin squeezing can only be induced by the presence of a transverse field. In Fig. 2 we plot the numerically calculated ground state squeezing parameter ξ as functions of the normalized transverse field strength H_x/N and the dipolar interaction strength c for $c_2>0$. The squeezing parameter shows plenty of features and squeezing occurs over a large parameter space explored. First one can notice that $\xi=1$ when $c=0$. Thus the ground state of a non-dipolar spinor condensate is not spin squeezed. Focusing on the region near $H_x=0$, we can easily identify two extrema of ξ at $c=1$ and $c=-0.5$. These two points correspond exactly to the boundaries between different quantum phases (see Fig. 1). The saturation fields in regions B and C can also be identified as they correspond to the local minima of ξ (dashed and solid lines in Fig. 2). The fact that the quantum phase boundaries are correlated with the extremum values of ξ is not a coincidence. Recent studies have shown that the bipartite concurrence (a measure of entanglement that is closely related to spin squeezing) also reaches extremum at the critical points of quantum phase transitions in many spin systems [20]. However, a full understanding of spin squeezing and entanglement in critical quantum systems is still lacking. With its rich quantum phases and the tunability of dipolar interaction strength, the dipolar spinor condensate appears to be an ideal system to address this problem.

V. DYNAMICAL MAGNETIZATION

The dynamic response of quantum spin systems to a time-dependent field represents another important magnetic property [21–23]. Here we will focus on the condensate in region B. Suppose the system is initially prepared under a weak transverse field H_x and a sufficiently strong longitudinal field H_z along the negative z-axis which polarizes the system into the state $|N,-N\rangle$. We then sweep the H_z from negative to positive value with a constant rate $v=dH_z/dt$. The typical energy spectrum is presented in the inset of Fig. 3. Without transverse field, the level $|N,-N\rangle$ (the ground state for $H_z<0$) crosses sequentially with $|N,N-k\rangle$ $(k=0,1,2,\ldots)$ at

$$H_z^{(k)} = -3ck.$$

The presence of H_x, however, changes the level-crossing at $H_z^{(k)}$ into anti-crossing by introducing a coupling between

levels $|N,-N\rangle$ and $|N,N-k\rangle$. The anti-crossings are characterized by the energy gaps $\Delta\varepsilon_k$ which can be found numerically. $\Delta\varepsilon_k$ increases with the transverse field H_x and the index k. According to the Landau-Zener formula [21,24], during the sweep of the longitudinal field, when the anti-crossing at $H_z^{(k)}$ is encountered, the system, initially on level $|N,-N\rangle$, has a probability of

$$p_k = \exp\left\{-\frac{\pi(\Delta\varepsilon_k)^2}{2(2N-k)v}\right\},$$

to stay on level $|N,-N\rangle$ and a probability of $1-p_k$ to jump to the state $|N,N-k\rangle$. The Landau-Zener transition, therefore, manifests in a series of jumps in the magnetization $\langle\hat{L}_z\rangle$ as shown in Fig. 3 where the results are obtained by numerically evolving the initial state under the Hamiltonian (7). As the field sweeps over the anti-crossings, the condensate wave function bifurcates into the states forming the anti-crossing and thus becomes a coherent superposition of states with different magnetization. This coherent superposition is the cause for the fast oscillations in the magnetization curve shown in Fig. 3. The size of the jumps matches well with those calculated from the transition probability using the Landau-Zener formula using the numerically obtained values of $\Delta\varepsilon_k$. A measurement of the position and the size of the jumps can thus be used to calibrate the field strengths along both the longitudinal and the transverse directions; or conversely, if the field strengths are known, one can obtain the value of c from such a measurement.

VI. MACROSCOPIC SPIN ENTANGLEMENT

Finally, we propose a scheme to create maximally entangled spin states using condensate in region B. Entanglement is an important feature of composite quantum systems, having application in quantum information and computation besides its importance for the foundations of quantum mechanics. There exist several proposals for creating entangled atomic state using spinor condensates [25]. Our scheme is illustrated in Fig. 4(a). First we prepare the condensate under a large transverse field $H_x > H_{\rm sat}$ such that the initial state is fully polarized along x-axis. The corresponding energy curve $E(\vartheta)$ [Eq. (8)] has a single minimum at $\vartheta=\pi/2$. We then slowly reduce H_x, for $H_x < H_{\rm sat}$, the single minimum splits into two degenerate ones symmetrically situated about $\vartheta=\pi/2$, and the state of the system becomes the symmetric quantum superposition of the two corresponding minimal energy states. When the field strength is further reduced to zero, the two minimal energy states become $|N,\pm N\rangle$ and the corresponding state of the system is the maximally spin entangled generalized N-body GHZ state

$$|\mathrm{GHZ}\rangle = \frac{1}{\sqrt{2}}(|N,N\rangle + |N,-N\rangle).$$

A direct numerical integration with the full Hamiltonian confirms this situation as demonstrated by Fig. 4(b) where the overlap between the generated state and the maximally entangled state $|\mathrm{GHZ}\rangle$ is plotted as a function of H_x. Compared to other entanglement generating schemes, ours possesses several distinct advantages: (1) The system remains in the minimal energy state throughout the whole process, making it immune from the spontaneous emission induced decoherence suffered by the electronically excited states; (2) this scheme does not rely on a precise knowledge of system parameters such as particle numbers, interaction strengths, and time; and (3) our scheme is rather robust, in the sense that when adiabaticity is not strictly obeyed, the final state may have slightly different weights on $|N,N\rangle$ and $|N,-N\rangle$, but remain significantly entangled. In addition, the adiabaticity requires a slow sweep only near the immediate vicinity at $H=H_{\rm sat}$. Away from this regime, a faster sweep can be adopted in order to decrease the total time duration. We note that our scheme also applies to other uniaxial magnetic materials.

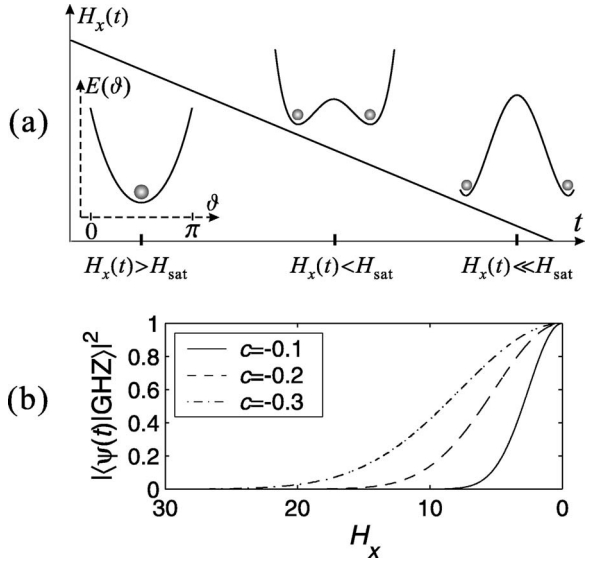

FIG. 4. The scheme for creating entangled atomic state. (a) Field strength H_x as a function of time. (b) The field dependence of the overlap of the condensate wave function with the maximally entangled state $|\mathrm{GHZ}\rangle$ for $N=20$ and a linear field sweeping rate $dH_x/dt=-0.06$.

VII. CONCLUSION

In conclusion, we have investigated the magnetic response of a dipolar spin-1 condensate. Specifically, we have studied the ground state phase structure and its relation to spin squeezing, the magnetization curves as well as the entanglement generation under a sweeping field. These studies give a taste of rich variety of static and dynamic phenomena displayed by dipolar spinor condensates. Our results show that the high tunability of this system makes it ideally suitable for studying quantum magnetism, quantum phase transition and other related phenomena.

ACKNOWLEDGMENT

This work is supported by the Oak Ridge Associated Universities and Rice University.

APPENDIX: DERIVATION OF THE HAMILTONIAN UNDER THE SMA

In this Appendix, we will show how the Hamitonian (4) is derived under the SMA. In the absence of dipolar interaction, the Hamiltonian of a spin-1 condensate under the SMA was derived by Law *et al.* [7] as

$$\mathcal{H}_0 = c_2'(\hat{\mathbf{L}}^2 - 2\hat{N}), \tag{A1}$$

where $\hat{N}$ is the total atom number operator. Here we outline the derivation of the dipole-dipole interaction Hamiltonian under the SMA. Putting the decomposition (3) into the dipolar Hamiltonian (2), we have

$$\begin{aligned}\mathcal{H}_{\mathrm{dd}} &= \frac{c_d}{2}\int d\mathbf{r}\int d\mathbf{r}'\frac{|\phi(\mathbf{r})|^2|\phi(\mathbf{r}')|^2}{|\mathbf{r}-\mathbf{r}'|^3}[(\hat{\mathbf{L}}^2 - 3(\hat{\mathbf{L}}\cdot\mathbf{e})^2) - (2\hat{N} - 3\hat{a}_\alpha^\dagger \mathbf{F}_{\alpha\beta}\cdot\mathbf{e}\mathbf{F}_{\beta\beta'}\cdot\mathbf{e}\hat{a}_{\beta'})] \\ &= \frac{c_d}{2}\int d\mathbf{r}\int d\mathbf{r}'\frac{|\phi(\mathbf{r})|^2|\phi(\mathbf{r}')|^2}{|\mathbf{r}-\mathbf{r}'|^3}\Bigg[\hat{L}_z^2(1-3\cos^2\theta_{\mathbf{e}}) - \frac{1}{4}(\hat{L}_+\hat{L}_- + \hat{L}_-\hat{L}_+)(1-3\cos^2\theta_{\mathbf{e}}) - \frac{3}{2}(\hat{L}_+\hat{L}_z\cos\theta_{\mathbf{e}}\sin\theta_{\mathbf{e}}e^{-i\varphi_{\mathbf{e}}} + \mathrm{H.c.}) \\ &\quad - \frac{3}{2}(\hat{L}_-\hat{L}_z\cos\theta_{\mathbf{e}}\sin\theta_{\mathbf{e}}e^{i\varphi_{\mathbf{e}}} + \mathrm{H.c.}) - \frac{3}{4}(\hat{L}_+^2\sin^2\theta_{\mathbf{e}}e^{-2i\varphi_{\mathbf{e}}} + \mathrm{H.c.}) + \hat{a}_0^\dagger\hat{a}_0(1-3\cos^2\theta_{\mathbf{e}}) - \frac{1}{2}(\hat{a}_1^\dagger\hat{a}_1 + \hat{a}_{-1}^\dagger\hat{a}_{-1})(1-3\cos^2\theta_{\mathbf{e}}) \\ &\quad + \frac{3}{\sqrt{2}}(\cos\theta_{\mathbf{e}}\sin\theta_{\mathbf{e}}e^{i\varphi_{\mathbf{e}}}\hat{a}_0^\dagger\hat{a}_1 + \mathrm{H.c.}) - \frac{3}{\sqrt{2}}(\cos\theta_{\mathbf{e}}\sin\theta_{\mathbf{e}}e^{-i\varphi_{\mathbf{e}}}\hat{a}_0^\dagger\hat{a}_{-1} + \mathrm{H.c.}) + \frac{3}{2}(\sin^2\theta_{\mathbf{e}}e^{2i\varphi_{\mathbf{e}}}\hat{a}_{-1}^\dagger\hat{a}_1 + \mathrm{H.c.})\Bigg],\end{aligned} \tag{A2}$$

where $\hat{L}_\pm \equiv \hat{L}_x \pm i\hat{L}_y$, $\theta_{\mathbf{e}}$ and $\varphi_{\mathbf{e}}$ are the polar and azimuthal angles of $(\mathbf{r}-\mathbf{r}')$, respectively. For an axially symmetric mode function $\phi(\mathbf{r})$, all terms involving $e^{\pm im\varphi_{\mathbf{e}}}$ vanish after integrating over $\varphi_{\mathbf{e}}$. $\mathcal{H}_{\mathrm{dd}}$ thus simplifies to

$$\mathcal{H}_{\mathrm{dd}} = c_d'(-\hat{\mathbf{L}}^2 + 3\hat{L}_z^2 + 3\hat{n}_0 - \hat{N}), \tag{A3}$$

with c_d' defined as in Eq. (6). One can then easily obtain the Hamiltonian (4) as the sum of $\mathcal{H}_0$ and $\mathcal{H}_{\mathrm{dd}}$, after dropping the terms dependent only on $\hat{N}$ which is a constant of motion. The presence of the $\hat{n}_0$ in the dipolar Hamiltonian (A3) breaks the conservation of total angular momentum $\hat{\mathbf{L}}^2$, but the projection along the z-axis, $\hat{L}_z$, is still conserved.

If the trapping potential and hence the mode function $\phi(\mathbf{r})$ do not possess the axial symmetry, then we must retain all the terms in Eq. (A2). When this is the case, the magnetization $\hat{L}_z$ is no longer a constant of motion. In addition, if the single mode approximation is not valid, then the terms neglected in arriving at Eq. (A3) may have to be kept even when the trapping potential is axisymmetric. This occurs, for example, when different spin components possess different orbital angular momenta. The case beyond the SMA will be published elsewhere.

[1] D. M. Stamper-Kurn, M. R. Andrews, A. P. Chikkatur, S. Inouye, H. J. Mesner, J. Stenger, and W. Ketterle, Phys. Rev. Lett. **80**, 2027 (1998).

[2] J. Stenger *et al.*, Nature (London) **396**, 345 (1998).

[3] M. Barret, J. Sauer, and M. S. Chapman, Phys. Rev. Lett. **87**, 010404 (2001).

[4] H. Pu, S. Raghavan, and N. P. Bigelow, Phys. Rev. A **61**, 023602 (2000); T.-L. Ho and S. K. Yip, Phys. Rev. Lett. **84**, 4031 (2000); M. Koashi and M. Ueda, *ibid.* **84**, 1066 (2000); Q. Gu, Phys. Rev. A **68**, 025601 (2003); Q. Gu and R. A. Klemm, *ibid.* **68**, 031604(R) (2003).

[5] T.-L. Ho, Phys. Rev. Lett. **81**, 742 (1998).

[6] T. Ohmi and K. Machida, J. Phys. Soc. Jpn. **67**, 1822 (1998).

[7] C. K. Law, H. Pu, and N. P. Bigelow, Phys. Rev. Lett. **81**, 5257 (1998).

[8] H. Schmaljohann, M. Erhard, J. Kronjager, M. Kottke, S. van Stea, L. Cacciapuoti, J. J. Arlt, K. Bongs, and K. Sengstock, Phys. Rev. Lett. **92**, 040402 (2004); M.-S. Chang, C. D. Hamley, M. D. Barrett, J. A. Sauer, K. M. Fortier, W. Zhang, L. You, and M. S. Chapman, *ibid.* **92**, 140403 (2004); J. Kronjäger *et al.*, cond-mat/0509083 (2005); M.-S. Chang *et al.*, cond-mat/0509341 (2005).

[9] S. Yi, L. You, and H. Pu, Phys. Rev. Lett. **93**, 040403 (2004).

[10] See, for example, M. Baranov *et al.*, Phys. Scr., T **102**, 74 (2002), and references therein.

[11] H. Pu, W. Zhang, and P. Meystre, Phys. Rev. Lett. **87**, 140405 (2001); W. Zhang, H. Pu, C. Search, and P. Meystre, Phys. Rev. Lett. **88**, 060401 (2002); H. Pu, W. Zhang, and P. Meystre, *ibid.* **89**, 090401 (2002); K. Gross, C. P. Search, H. Pu, W. Zhang, and P. Meystre, Phys. Rev. A **66**, 033603 (2002).

[12] A. Griesmaier, J. Werner, S. Hensler, J. Stuhler, and T. Pfau,

Phys. Rev. Lett. **94**, 160401 (2005).
[13] L. Santos and T. Pfau, cond-mat/0510634 (2005); Y. Kawaguchi, H. Saito, and M. Ueda, e-print cond-mat/0511052 (2005); R. B. Diener and T.-L. Ho, e-print cond-mat/0511751 (2005).
[14] S. Yi, O. E. Mustecaplioğlu, C. P. Sun, and L. You, Phys. Rev. A **66**, 011601 (2002).
[15] E. M. Chudnovsky, *Macroscopic Quantum Tunneling of the Magnetic Moment* (Cambridge University Press, Cambridge, 1998).
[16] D. J. Wineland, J. J. Bollinger, W. M. Itano, F. L. Moore, and D. J. Heinzen, Phys. Rev. A **46**, R6797 (1992).
[17] M. Kitagawa and M. Ueda, Phys. Rev. Lett. **67**, 1852 (1991); Phys. Rev. A **47**, 5138 (1993).
[18] A. Sørensen *et al.*, Nature (London) **409**, 63 (2001).
[19] O. Müstecaplioğlu, M. Zhang, and L. You, Phys. Rev. A **66**, 033611 (2002).
[20] A. Osterloh *et al.*, Nature (London) **416**, 608 (2002); T. J. Osborne and M. A. Nielsen, Phys. Rev. A **66**, 032110 (2002); X. Wang and B. C. Sanders, *ibid.* **68**, 012101 (2003); J. Vidal, G. Palacios, and R. Mosseri, *ibid.* **69**, 022107 (2004); S. Gu, S. S. Dang, Y. Q. Li, and H. Q. Lin, Phys. Rev. Lett. **93**, 086402 (2004).
[21] S. Miyashita, J. Phys. Soc. Jpn. **64**, 3207 (1995).
[22] J. R. Friedman, M. P. Sarachik, J. Tejada, and R. Ziolo, Phys. Rev. Lett. **76**, 3830 (1996); J. M. Hernández *et al.*, Europhys. Lett. **35**, 301 (1996); L. Thomas *et al.*, Nature (London) **383**, 145 (1996); W. Wernsdorder and R. Sessoli, Science **284**, 133 (1999).
[23] H. De Raedt, S. Miyashita, K. Saito, D. Garcia-Pablos, and N. Garcia, Phys. Rev. B **56**, 11761 (1997); E. Rastelli and A. Tassi, *ibid.* **64**, 064410 (2001).
[24] C. Zener, Proc. R. Soc. London, Ser. A **137**, 696 (1932).
[25] H. Pu and P. Meystre, Phys. Rev. Lett. **85**, 3987 (2000); L.-M. Duan, A. Sorensen, J. I. Cirac, and P. Zoller, *ibid.* **85**, 3991 (2000); L. You, *ibid.* **90**, 030402 (2003); M. Zhang and L. You, *ibid.* **91**, 230404 (2004).